Clim. Past Discuss., 8, 5455–5492, 2012
www.clim-past-discuss.net/8/5455/2012/
doi:10.5194/cpd-8-5455-2012

Climate of the Past Discussions

On the origin of multi-decadal to centennial Greenland temperature anomalies over the past 800 yr

T. Kobashi[1,2], D. T. Shindell[3], K. Kodera[4,5], J. E. Box[6,7], T. Nakaegawa[4], and K. Kawamura[1]

[1]National Institute of Polar Research, 10-3 Midoricho, Tachikawa, Tokyo, 190-8518, Japan
[2]Scripps Institution of Oceanography, University of California, San Diego, La Jolla, California, 92093, USA
[3]NASA Goddard Institute for Space Studies, New York, New York, 10025, USA
[4]Meteorological Research Institute, Tsukuba, 305-0052, Japan
[5]Solar Terrestrial Environment Laboratory, Nagoya University, Nagoya, Japan
[6]Byrd Polar Research Center, The Ohio State University, Columbus, Ohio, 43210, USA
[7]Department of Geography, The Ohio State University, Columbus, OH 43210, USA

Received: 28 September 2012 – Accepted: 3 November 2012 – Published: 8 November 2012

Correspondence to: T. Kobashi (kobashi.takuro@nipr.ac.jp)

Published by Copernicus Publications on behalf of the European Geosciences Union.

Abstract

The surface temperature of the Greenland ice sheet is among the most important climate variables for assessing how climate change may impact human societies associated with accelerating sea level rise. However, the causes of multi-decadal-to-centennial temperature changes in Greenland are not well understood, largely owing to short observational records. To examine the causes of the Greenland temperature variability, we calculated the Greenland temperature anomalies ($GTA_{(G\text{-}NH)}$) over the past 800 yr by subtracting the standardised NH temperature from the standardised Greenland temperature. It decomposes the Greenland temperature variation into background climate (NH); Polar amplification; and Regional variability ($GTA_{(G\text{-}NH)}$). The Central Greenland polar amplification factor as expressed by the variance ratio = Greenland/NH is 2.6 over the past 161 yr, and 3.3–4.2 over the past 800 yr. The GTA explains 31–35 % of the variation of Greenland temperature in the multi-decadal-to-centennial time scale over the past 800 yr. Another orthogonal component of the Greenland and NH temperatures, $GTP_{(G+NH)}$ (Greenland temperature plus = standardized Greenland temperature + standardized NH temperature) exhibited the multi-decadal variations that were likely induced by large volcanic eruptions, increasing greenhouse gasses, and internal variation of climate. We found that the $GTA_{(G\text{-}NH)}$ has been influenced by solar-induced changes in atmospheric circulation patterns such as those produced by North Atlantic Oscillation/Arctic Oscillation (NAO/AO). Climate modelling indicates that the anomaly is also likely linked to solar-paced changes in the Atlantic meridional overturning circulation (AMOC) and to associated changes in northward oceanic heat transport.

1 Introduction

The surface air temperature over Greenland is known to be affected by large volcanic eruptions, changes in solar output, anthropogenic influences and the North Atlantic

CPD
8, 5455–5492, 2012

Oscillation (NAO) and/or the Atlantic Multi-decadal Oscillation (AMO) (Box et al., 2009; Hanna and Cappelen, 2003; Vinther et al., 2003; Hurrell, 1995). These regional variations have caused Greenland temperature to depart from the baseline trend defined by the average temperature of the Northern Hemisphere (NH) (Box et al., 2009). For more accurate projections of the future mass balance of the Greenland ice sheet and of sea level changes, it is critical to understand the mechanisms underlying Greenland surface temperature changes.

Greenland surface temperature, especially the temperature in Western Greenland, fluctuates in a manner inversely related to the observed spatial pattern of the NAO (Hanna and Cappelen, 2003; Box et al., 2009; Vinther et al., 2003). The NAO, an important mode of climate variability in the North Atlantic that influences North Africa, Europe and North America particularly in the winter is often represented by the difference in sea level pressure between the Azores high and the Icelandic low (Hurrell, 1995). Recent studies have shown that NAO variability is closely linked to changes in the atmospheric blocking regime, which constitutes quasi-stationary anticyclonic systems interrupting the normal zonal flow (Woollings et al., 2010; Barriopedro et al., 2008; Rimbu and Lohmann, 2011; Häkkinen et al., 2011). When the NAO index is positive, West Greenland temperature decreases due to stronger northerly winds, whereas Northwestern Europe experiences warmer temperatures in response to stronger westerlies, and when the NAO index is negative, the opposite effects are observed (Wanner et al., 2001). An influence of the NAO on the average NH temperatures has also been suggested (Hurrell, 1996). Climate models (Shindell et al., 2001) and observations (Kodera, 2002; Ineson et al., 2011) indicate a link between NAO-like variability and changes in solar output (Gray et al., 2010).

During periods of stronger solar activity, ozone in the upper stratosphere and lower mesosphere absorb the increased ultraviolet irradiance, which increases the ambient temperature. Higher ultraviolet irradiance also increases ozone production through the photodissociation of molecular oxygen in the stratosphere (Haigh, 1999). As the temperature signal is maximized in the tropical latitudes as the result of this process,

CPD
8, 5455–5492, 2012

the temperature gradients between the low and high latitudes in the stratosphere are amplified, creating stronger tropospheric westerly winds and associated pressure and temperature fields at the surface, resembling positive NAO-like atmospheric patterns (Kodera and Kuroda, 2002; Shindell et al., 2001). During periods of lower solar activity such as the Maunder Minimum, climate models and proxy records both suggest negative NAO-like patterns and warm Southwest Greenland temperature anomalies (Shindell et al., 2001). The spatial pattern of climate change from the Medieval Warm Period to the Little Ice Age was shown to possess some features resembling to the solar-induced NAO/AO pattern (Mann et al., 2009).

In this study, we investigated the variations in the Greenland temperature anomaly using a recently developed Greenland temperature record (Kobashi et al., 2010, 2011) derived from trapped air in the GISP2 Greenland ice core from the Greenland Summit station and using two proxy average NH temperature reconstructions (Mann et al., 2009; Moberg et al., 2005). Proposed mechanisms for the temperature variations were then investigated with a climate model (GISS-ER) and proxy grid temperature reconstructions (Mann et al., 2009).

2 Observational period (1850–2010)

We first investigated the Greenland near-surface air temperature trend in the vicinity of the Summit station (72° 35′ N, 38° 27′ W) during the 1850–2010 period based on a spatial-temporal data fusion of observed temperature records and regional climate model output (Box et al., 2009). Uncertainties of the temperature record in earlier periods are likely larger as observational constrains are limited (Box et al., 2009). We compared this trend with the average temperatures of the NH (HadCRUT3) (Brohan et al., 2006) (Fig. 1). We noted that the Summit air temperature is highly correlated ($r = 0.92$, $p < 0.01$; Fig. 2) with the average surface air temperature of the entire Greenland ice sheet (Box et al., 2009; Kobashi et al., 2011) indicating that the Summit temperatures reconstructed from ice cores are a reliable proxy for the surface temperature

CPD
8, 5455–5492, 2012

trend of the entire ice sheet. Hereinafter, we call the Summit temperature time series "Greenland temperature". Furthermore the reconstructed Summit temperature for the 1855–2010 period is significantly correlated ($r = 0.77$, $p < 0.01$) with the long record of observed temperatures from the Iluissat settlement (Cappelen, 2011) located on the west coast of Greenland.

The Greenland and NH average temperatures over the past 161 yr follow similar trends ($r = 0.66$, $p = 0.17$; after liner detrending $r = 0.47$, $p = 0.09$) but with noticeable differences (Box et al., 2009) (Fig. 1; top panel). Differences in the temperature trends for Greenland and the NH at the decadal scale include stronger Greenland warming during the decade 1920–1930, decades-long cooling during the 1930s–1980s, and another warming episode in the 1990s and 2000s all with similar magnitudes (Fig. 1). As a result, the decadal average temperatures in Greenland in the 1930s and 2000s are of similar magnitude (Fig. 1) as found also in glacial extents (Bjørk et al., 2012). Unlike in Greenland, the NH temperature during the last decade (2001–2010) was the warmest for the observed period (Fig. 1). To examine why Greenland temperature deviates from the NH temperature trend, we calculated the Greenland temperature anomaly ($GTA_{(G\text{-}NH)}$) by subtracting the standardised NH temperatures from the standardised Greenland temperatures (Fig. 1) (see Appendix A). This calculation allowed us to decompose Greenland temperature variation into three factors: background climate (NH); polar amplification; and regional variability ($GTA_{(G\text{-}NH)}$). The Central Greenland polar amplification factor as expressed by the variance ratio = Greenland/NH is 2.6 over the past 161 yr.

Near-surface air temperatures in much of Greenland's area exhibits a negative correlation with the NAO index especially in winter (Box, 2002). As annual temperature variability is dominated by winter temperature variability in Greenland (Vinther et al., 2010), we hypothesize that the variation in the $GTA_{(G\text{-}NH)}$ is linked to the NAO/AO. Indeed, the $GTA_{(G\text{-}NH)}$ is negatively correlated with the NAO index (averages of the winter NAO; DJFM) (Jones et al., 1997; Osborn, 2011) with a 94 % confidence level ($r = -0.44$, $p = 0.06$; for the 1960–2007 with 3-yr running means (RMs); Fig. 1) over

CPD
8, 5455–5492, 2012

the past 48 yr. Cooling signals associated with large volcanic eruptions are known to be similar to cooling signals of weaker solar activity, which makes it difficult to differentiate solar and volcanic signals (Lean and Rind, 2008; Gray et al., 2010). However, solar signals are out-of-phase between the NH and Greenland temperatures (cooling in NH and warming in Greenland, and vice versa), but volcanic signals are in-phase between the NH and Greenland temperatures (cooling in NH and Greenland) providing a rare opportunity to differentiate the two natural climate forcings.

The inter-annual variations of the $GTA_{(G\text{-}NH)}$ correlates weakly but significantly with the 11-yr solar cycle over the past 48 yr ($r = -0.29$, $p = 0.09$ for the 1960–2007 period) (Fig. 1, middle panel; however, the correlation is not significant – $r = -0.27$, $p = 0.35$; Appendix A – for the entire observational period 1851–2007). The inconsistency may relate to the empirical findings that climate is more sensitive to the solar forcing at the multidecadal-to-century time scale than shorter variations of solar activity such as the 11-yr solar cycle (Waple et al., 2002; Gray et al., 2010). In the multi-decadal-to-centennial time scale, the $GTA_{(G\text{-}NH)}$ indicates an increasing trend until the 1930s. Note the $GTA_{(G\text{-}NH)}$ vertical axis is reversed in Fig. 1. The $GTA_{(G\text{-}NH)}$, thereafter showed a decreasing trend, indicating that Greenland temperature decreased relative to that of the NH until ~ 1990. Then, the $GTA_{(G\text{-}NH)}$ increased to the present associated with more rapid warming in Greenland than that in the NH (Fig. 1). The multi-decadal trend of the $GTA_{(G\text{-}NH)}$ is similar to the long-term variation of solar activity over the past 160 yr (Fig. 1) with a possible lag of 20–30 yr. However, the observational records are too short to support a causal relationship between the solar variability and the $GTA_{(G\text{-}NH)}$ in the multi-decadal-to-centennial time scale.

3 The past 800 yr of Greenland temperature anomaly ($GTA_{(G\text{-}NH)}$)

To evaluate the robustness of the apparent solar influence on the multi-decadalto-centennial $GTA_{(G\text{-}NH)}$ variation, we examined records for the past 800 yr (Fig. 3). For Greenland temperature, we used a recently developed record of the temperature at

CPD
8, 5455–5492, 2012

Summit that was reconstructed (see Appendix B) from air trapped in the GISP2 ice core (Kobashi et al., 2010). Owing to gas and heat diffusion in the firn layer (porous unconsolidated snow), the temperature record represent decadal averages (Severinghaus et al., 1998). For the NH temperature, two proxy based reconstructions by Moberg et al. (2005) and Mann et al. (2009) were used (Fig. 3). The NH and Greenland temperatures exhibit similar trends with the characters of the Medieval Warm Period in 1200–1450 the Little Ice Age in 1450–1850, and recent warming (Fig. 3).

We then derived two 800-yr $GTAs_{(G\text{-}NH)}$ by the same method used for the observational records (Appendix A; Fig. 3). The two $GTAs_{(G\text{-}NH)}$ exhibit similar characteristics over the past 800 yr ($r = 0.79$, $p = 0.02$), indicating that the signal is a robust feature of the $GTA_{(G\text{-}NH)}$. The $GTAs_{(G\text{-}NH)}$ explains 31–35 % of the variation of Greenland temperature over the past 800 yr. The Central Greenland polar amplification factor (= Greenland/NH) over the past 800 yr range from 3.3 for the NH temperature from Moberg et al. (2005) to 4.2 for the NH temperature from Mann et al. (2009) The $GTAs_{(G\text{-}NH)}$ show more negative values (with Greenland being cooler than the NH) before 1400 and after 1700 and positive values (with Greenland being warmer than the NH) between 1400 and 1700, indicating that there was a more positive NAO-like pattern before 1400 and after 1700 and a more negative pattern in the intervening period The persistent positive NAO during the Medieval Warm Period is consistent with the results of a recent study (Trouet et al., 2009).

To investigate the relationship between the $GTA_{(G\text{-}NH)}$ and changes in solar activity over the past 800 yr, we used two solar forcing reconstructions based on ^{10}Be in ice cores from Antarctica (Bard et al., 1997; Crowley, 2000). Wavelet analyses revealed that Greenland temperature has a weak anti-phase correlation with the TSI (Fig. 4) around the period (~ 128 yr). In contrast, the NH temperature generally exhibits a weak in-phase relationship with the TSI over the past 800 yr (Fig. 4). As a result, solar signals are enhanced in the $GTA_{(G\text{-}NH)}$ and exhibits significant anti-phase with the TSI especially around the period of ~ 128 yr (Fig. 4).

CPD
8, 5455–5492, 2012

To test the null hypothesis that solar variation did not cause changes in $GTAs_{(G\text{-}NH)}$ over the past 800 yr, we conducted a statistical "re-sampling" test. Periods of stronger and weaker solar output were defined according to the changes in TSI, and differences of the means of the $GTA_{(G\text{-}NH)}$ for the stronger and weaker solar periods were calculated. Statistical significance of the difference was tested using a Monte Carlo sampling considering uncertainties in the NH and the Greenland temperatures (see Appendix C). Then, we found that when solar output is strong (weak), the $GTA_{(G\text{-}NH)}$ is low (high) with a 98 % (with the NH temperature by Mann et al., 2009) or 99.9 % (with the NH temperature by Moberg et al., 2005) confidence levels over the past 800 yr. One caveat for the calculation of the $GTA_{(G\text{-}NH)}$ from Greenland temperature and the NH temperature is that the correlation of the $GTA_{(G\text{-}NH)}$ with solar activity may arise entirely from the correlation between the NH temperatures and solar activity. We tested the null hypothesis by examining contributions of correlations from the Greenland and the NH temperatures on $GTA_{(G\text{-}NH)}$ with solar activity (see Appendix D), and the hypothesis was rejected at the 99.9 % significance level, indicating that the changes in solar activity induced negative variations in Greenland temperature and positive variations in the NH temperature (see Appendix D). The finding is also consistent with the fact that the Greenland temperature has a weak but significant negative correlation with solar activity over the past 4000 yr (Kobashi et al., 2012) (Fig. 5).

We conducted a simple numerical experiment to further test the validity of finding solar signals from the $GTA_{(G\text{-}NH)}$ calculation (see Appendix E for details of the calculation). First, we note that the $GTA_{(G\text{-}NH)}$ is one of the principal components of the Greenland and the NH temperatures. Another orthogonal component of the two time series, "$GTP_{(G+NH)}$" (Greenland temperature plus = standardized Greenland temperature + standardized NH temperature), should represent the NH temperature trend from which climate responses to multi-decadal-to-centennial solar variations are removed (Fig. 6). This is because solar signals in the Greenland temperature and the NH temperature seen as the $GTA_{(G\text{-}NH)}$ should be cancelled by combining the two time series. As a result, the $GTP_{(G+NH)}$ variation (Fig. 6, top) in the multi-decadal-to-centennial

CPD
8, 5455–5492, 2012

time scale likely reflects changes in volcanic forcing increasing greenhouse gas forcing since ~ 1850 and possibly internal variation of climate. Millennialscale variation (Fig. 6, top) of the $GTP_{(G+NH)}$ peaking in the 1300s and 1700s may reflect non-linear climate responses to solar and/or volcanic forcing.

Combining the millennial trend, solar forcings, and random noises, we produced synthetic NH temperatures (Fig. 6, middle). Then, synthetic Greenland temperatures were produced by adding negative solar signals on the synthetic NH temperatures (Fig. 6, middle, see Appendix E). Residuals between the model results and the observations (2σ values are 1.6 for the standardized Greenland temperatures and 1.2 for the standardized NH temperatures as in Fig. 6, middle) are smaller than the long term changes (3 for the standardized Greenland temperatures; 2.7 for the standardized NH temperatures as in Fig. 6 middle) support the validity of the model. The synthetic $GTA_{(G-NH)}$ from the synthetic Greenland and the synthetic NH temperatures captures the original solar signal ($r = -0.83$) with slightly different features. The synthetic $GTA_{(G-NH)}$ show slightly higher correlation ($r = 0.59$) with the observed $GTA_{(G-NH)}$ than the correlation ($r = -0.55$) with the original solar signal (Fig. 6), indicating that the $GTA_{(G-NH)}$ calculation introduces a minor alteration on solar signal as in Fig. 6. We confirmed also that the synthetic $GTP_{(G+NH)}$ can fully recover the millennial trend ($r > 0.99$). In addition, the synthetic $GTA_{(G-NH)}$ calculated with synthetic NH temperature without solar signal (the trend and noises only) and synthetic Greenland temperature (with negative solar signal) is more strongly correlated with the original solar signals, indicating that the observed correlation between the solar forcing and the $GTA_{(G-NH)}$ is not an artifact of solar signal in the NH temperature.

4 Climate model experiments

We examined the climate model responses of the $GTAs_{(G-NH)}$ in a coupled atmosphere-ocean climate model (see Appendix F), the NASA Goddard Institute for Space Studies–ER (GISS-ER) simulation (Mann et al., 2009; Schmidt et al., 2006). Six GISS-ER

CPD
8, 5455–5492, 2012

transient runs were conducted for the 850–1900 period (Mann et al., 2009) with solar forcing but without volcanic forcing. Solar forcing based on ^{10}Be data from an ice core from the South Pole (Bard et al., 2007) was calibrated using the TSI (Mann et al., 2009) (see Appendix F). The model includes parameterised ozone responses to solar irradiance variations in the atmosphere (Schmidt et al., 2006). The $GTAs_{(G\text{-}NH)}$ in the model were calculated using the average temperature of Southern Greenland including the GISP2 site as the northern limit (72° 36′ N, 38° 30′ W; 3200 m a.s.l.). The ensemble averages of the six $GTAs_{(G\text{-}NH)}$ calculated with GISS-ER model were compared with the changes in solar irradiance (Fig. 7), and a similar correlation ($r = -0.47$, ranging from $r = 0.11$ to -0.75 in individual runs) to the observation was found between the $GTA_{(G\text{-}NH)}$ and solar variability in the multi-decadaltocentennial timescale (e.g. 51-yr RMs; Fig. 7). The re-sampling test indicated a significant solar influence on the $GTA_{(G\text{-}NH)}$ variation in the GISS-ER model in a 97 % confidence level.

We also tested the null hypothesis that the correlation between the $GTA_{(G\text{-}NH)}$ and solar forcing in the model is a result of correlations between the NH temperature and the TSI. The null hypothesis was rejected for the $GTA_{(G\text{-}NH)}$ in the GISS-ER simulation, indicating Greenland temperature negatively responded to changes in solar activity (see Appendix D) Therefore the observed $GTA_{(G\text{-}NH)}$ variations including the negative correlation between Greenland temperature and solar forcing are physically explainable. This result is consistent with the results of earlier studies showing that the GISS simulation with integrated ozone feedback processes appears to properly reproduce solar-induced NAO/AO-like dynamics (Mann et al., 2009).

5 Dynamic causes of solar induced $GTA_{(G-NH)}$ variation

To investigate the spatial extent and mechanisms of solar-induced $GTA_{(G\text{-}NH)}$ variations, we plotted the composite-mean temperature differences of periods of stronger and weaker solar output, as defined in Fig. 3 for the model outputs and the grid proxy temperature reconstruction (Mann et al., 2009) (Fig. 8). Importantly, the spatial features

CPD
8, 5455–5492, 2012

in the proxy map resemble the surface air temperature responses to the 11-yr solar cycles for the 1889–2006 period (Lean and Rind, 2008). The locations and extents of small areas of cooling in the Northern North Atlantic are consistent in the two maps (Fig. 8). The cooling signal cannot be a result of the contamination of volcanic signals as large volcanic events were observed to cause positive NAOs and thus an in-phase relationship between the NH and Greenland temperatures. In addition, note that the temperatures in Southern Greenland in the GISS-ER show cooler areas.

Earlier studies using the GISS-ER simulation and observations have shown that the NAO/AO-like temperature pattern is related to changes in large-scale dynamic atmospheric circulation (Lean and Rind, 2008) and polar night jets resulting primarily from solar spectral (UV) changes (Kuroda and Kodera, 2002; Kodera and Kuroda, 2002). Composite differences in the sea level pressure (SLP) in the GISS-ER model indicate significant pressure increases over both the Atlantic and Pacific sectors at mid-latitudes and decreases over the majority of the Northern high latitudes (Fig. 9). Although the SLP anomalies show a more complex structure than the NAO and AO patterns and the signals are rather weak, these changes do project onto both of those variability modes and lead to altered flow from North America towards Greenland and the North Atlantic similar to that induced by NAO/AO anomalies (Fig. 9). As a result Greenland experiences stronger northerly winds and resultant cooler temperatures. Earlier studies with GISS-ER and previous version of GISS have shown that the solar-induced NAO/AO-like patterns are amplified by the interactive ozone processes in the atmosphere (top-down process, Gray et al., 2010) as described previously (Mann et al., 2009; Shindell et al., 2001) and by a "bottom-up" process (Gray et al., 2010) linked to changes in solar activity (e.g. tropical and subtropical moisture convection processes through surface heating) (Shindell et al., 2001; Kodera, 2002; Kodera and Kuroda, 2002).

Regarding the observed centennial to multi-decadal variations in $GTAs_{(G\text{-}NH)}$, the mechanisms may involve oceanic processes such as the Atlantic meridional overturning circulation (AMOC) (Waple et al., 2002; Cubasch et al., 1997). To further investigate the dynamic causes of the $GTA_{(G\text{-}NH)}$ variations, we investigated changes in the

CPD
8, 5455–5492, 2012

AMOC. The GISS-ER simulation exhibits a significant reduction of 0.3 Sv (1.4 %) from the mean value of 21.1 Sv in the AMOC in response to stronger solar forcing, thus indicating slowed heat transport from the South to the North Atlantic, which may explain part of the anti-phase relationship between the NH and the Southern Greenland temperatures. The same AMOC processes are often observed in model projections of future warming (Meehl et al., 2007). Owing to reduced AMOC in many models, Northern North Atlantic areas including Northern Europe are projected to experience less warming. Therefore, the observed negative responses to solar variation in the Northern North Atlantic likely indicate that oceanic responses to changes in solar outputs played a role in the $GTA_{(G\text{-}NH)}$ variations.

6 Conclusions

Over the past 800 yr, Greenland temperature variability was dominated by background climate changes on the Northern Hemispheric scale, and these changes are known to be largely the result of solar and volcanic forcing prior to 1850 (Crowley, 2000). However, we find that the deviations in Greenland temperatures from that of the NH are also strongly influenced by atmospheric dynamics such as those produced by the NAO/AO in which longer-term variations are induced by variations in solar outputs with an additional contribution from the oceanic response. This finding indicates that Greenland temperature minimum over the past 800 yr occurred in the early 18th century contrasting to the minimum for the NH temperature in the 15–16th century (Figs. 3 and 6) – likely because of increased solar forcing during the 18th century. In addition, during the latter half of the 20th century, Greenland temperature exhibited less pronounced warming than the warming of the NH at the time of high solar activity. If future solar activity remains low compared with that of the past 100 yr (Livingston and Penn, 2009), it may reveal a hidden warming of Greenland caused by increasing greenhouse gasses during the latter half of the 20th century.

CPD
8, 5455–5492, 2012

Appendix A

Calculations of $GTA_{(G\text{-}NH)}$, filtering, correlation coefficients

We calculated the Greenland temperature anomaly ($GTA_{(G\text{-}NH)}$) from the NH trend for a period of 161 yr as follows. The variance of the inter-annual variability of the standardised Greenland temperature is higher than that of the standardised NH temperature over the past 161 yr, potentially affecting the longer-term variation of the $GTA_{(G\text{-}NH)}$. Therefore, a 3-yr running mean (RM) filter is applied to the raw data for Greenland temperature and the NH temperature to reduce the inter-annual variability, so the $GTA_{(G\text{-}NH)}$ reflects the decadal to multi-decadal temperature anomalies in Greenland temperature with respect to the NH temperature trend. After the filtering, the NH and Greenland temperature time series are standardised to calculate the $GTA_{(G\text{-}NH)}$. For the standardisation, we subtracted the average value from each time series and divided the time series by the standard deviation of the time series; the resulting time series had means of zero and standard deviations of one.

For the data over the past 800 yr, we initially applied 21 RMs to the NH and Greenland temperatures prior to standardisation to illustrate multi-decadal to centennial variability in the $GTA_{(G\text{-}NH)}$. We standardized the time series by subtracting the means and dividing the time series by the standard deviations, so the resulting time series have means of zero and standard deviations of 1. Ninety-five per cent confidence intervals for the NH (Mann et al., 2009) and Greenland (Kobashi et al., 2010) temperatures with 21 RMs were estimated by Monte Carlo simulation as follows. Gaussian white noise signals with a standard deviation of 1 and a mean of zero are generated and then multiplied by the reported 1σ values for the NH (Mann et al., 2009) and Greenland (Kobashi et al., 2010) temperature data for each year. These modified signals were then added to the original NH and Greenland temperature time series. By repeating this calculation 1000 times, 1000 synthetic NH and Greenland temperature time series were generated. For each time series, 21 RMs were applied. The 1σ values of the NH

CPD
8, 5455–5492, 2012

and Greenland temperature time series with the 21 RMs were then estimated from the 1000 synthetic time series.

To address the uncertainty in the NH temperatures in the 21 RMs of Moberg et al. (Moberg et al., 2005), we directly used the uncertainty due to the variance among low-resolution proxies (uncertainty A) (Moberg et al., 2005), but we did not include the uncertainty in the scaling factor (uncertainty B) (Moberg et al., 2005) or the constant adjustment term (uncertainty C) (Moberg et al., 2005) because these uncertainties were not relevant for standardising time series. The estimated 1σ values of the NH and Greenland temperatures with 21 RMs were scaled for the standardised NH and Greenland temperatures in 21 RMs using the same values for standardising the NH and Greenland temperatures with 21 RMs. The uncertainties in the $\mathrm{GTA}_{(\mathrm{G\text{-}NH})}$ were derived from the equation for the propagation of error: $\sigma\mathrm{GTA} = \sqrt{(\sigma\ \mathrm{stn.\ NH})^2 + (\sigma\ \mathrm{stan.\ Greenland})^2}$, where σGTA, σ stn. NH, and σ stn. Greenland are the standard deviations of the GTA, the standardised NH temperature, and the standardised Greenland temperature, respectively.

The Pearson product-moment correlation coefficient was calculated to evaluate the strength of a correlation. The number of effective degrees of freedom ($\mathrm{df_e}$) for p statistics was estimated from the effective sample size (N_e), which depends on the effective decorrelation time (T_e) (Ito and Minobe, 2010). The two relevant time series were represented by X and Y, and the sample size is N. Here, the time interval (Δt) was 1 yr. Therefore, $N_\mathrm{e} = N\Delta t/T_\mathrm{e}$ and $\mathrm{df_e} = N_\mathrm{e} - 2$. For the correlation coefficients, T_e were estimated as $T_\mathrm{e} = \Delta t \sum_{\tau=-N}^{N}(\rho_{XX}(\tau)\rho_{YY}(\tau) + \rho_{XY}(\tau)\rho_{YX}(\tau))$, where τ is a lag or a lead in years, and ρ is the correlation coefficient of the two time series indicted by the subscripts (XX and YY are autocorrelations) (Ito and Minobe, 2010). The range of Σ ($-N$, N) was defined as ρ became zero when changing τ starting from zero and moving to an increased lag or lead with a 1-yr time step.

CPD
8, 5455–5492, 2012

Appendix B

Description of reconstructed Greenland over the past 1000 yr

Recently, a precise Greenland Summit temperature record with strict age control was developed for the past 1000 yr, using argon and nitrogen isotope records from trapped air in the GISP2 ice core (Kobashi et al., 2008, 2010, 2011) This method addresses deficiencies in the existing Greenland temperature proxies, such as $\delta^{18}O_{ice}$ and borehole thermometry (Kobashi et al., 2011), providing decadal averages owing to gas diffusion in the firn (unconsolidated snow) layer; thus, this new temperature record is not affected by large seasonal temperature swings (Severinghaus et al., 1998). A strong correlation (as high as $r = 0.61$) with the Northern North Atlantic grid temperature data (Mann et al., 2009) is evident for the 1200–1993 period (Fig. A1).

Appendix C

Statistical testing (re-sampling) for the null hypothesis of the solar influence on the $GTA_{(G\text{-}NH)}$

We determined the periods of stronger and weaker solar output using two times series of solar forcing, as shown in Fig. 3. The two time series of solar forcing were smoothed by 21 RMs; and then standardized. The two resulting time series were averaged to generate a representative time series of solar forcing. We simply defined the periods of stronger solar output as periods when the standardized solar forcing was positive, and the periods of weaker solar output were defined as the periods when the standardized solar forcing was negative (Table A1). In total, there were 384 yr of stronger solar output, and 417 yr of weaker solar output.

We tested the null hypothesis that solar variation did not modulate the $GTA_{(G\text{-}NH)}$ over the past 800 yr using a statistical method for "re-sampling" (Ito and Minobe, 2010) as

CPD
8, 5455–5492, 2012

follows. First, the averages of the $GTA_{(G\text{-}NH)}$ corresponding to the periods of "stronger" and "weaker" solar output were calculated. The averages of the $GTA_{(G\text{-}NH)}$ for stronger and weaker solar output were then subtracted to obtain the average difference in the $GTA_{(G\text{-}NH)}$ between the periods of stronger and weaker output. Second, the order of the 11 durations in Table A1 was randomly shuffled. Based on the new order of the durations, 11 periods were calculated from 2000 C.E. to 1200 C.E. Periods of stronger and weaker solar output were defined as the odd and even numbers, respectively, in the new order. In addition, the assignments of odd and even numbers to periods of stronger and weaker solar output were randomly replaced. A synthetic $GTA_{(G\text{-}NH)}$ is generated by adding Gaussian white noise (with a zero mean and a standard deviation of 1) multiplied by the uncertainties (1σ) of the previously calculated $GTAs_{(G\text{-}NH)}$. The averages of the $GTAs_{(G\text{-}NH)}$ from the periods of stronger and weaker solar output were then calculated, and the difference between these two averages was calculated. This process was repeated 10 000 times (1000 times for maps) to generate a set of 10 000 samples (1000 samples for maps) for the differences. Percentile ranks were calculated and used to test the null hypothesis (one-sided test as we are only interested in Greenland cooling (warming) not warming (cooling) during stronger (weaker) sun, respectively) and to determine the significance levels of the observed differences in the $GTA_{(G\text{-}NH)}$ between periods of stronger and weaker solar output. We found that for the $GTA_{(G\text{-}NH)}$ with respect to the NH temperature of Moberg et al. (2005), the null hypothesis was rejected at the 99.9 % significance level, and for the $GTA_{(G\text{-}NH)}$ with the NH temperature of Mann et al., the null hypothesis was rejected at the 98 % confidence level. Therefore, we conclude that solar variability has caused changes in the $GTA_{(G\text{-}NH)}$ over the past 800 yr.

CPD
8, 5455–5492, 2012

Appendix D

Testing correlations between the $GTA_{(G\text{-}NH)}$ and solar variability

To test the null hypothesis that the correlations between the $GTA_{(G\text{-}NH)}$ and solar variability originate completely from the positive correlation between the NH temperature and solar variation, we conducted a statistical test by decomposing the standardized Greenland temperature ($\hat{T}_G$) and the standardized NH temperature ($\hat{T}_{GH}$) as follows:

$$T_a = (\hat{T}_G + \hat{T}_{GH})/\sqrt{2} \quad \text{(D1)}$$

$$T_b = (\hat{T}_G - \hat{T}_{GH})/\sqrt{2} \quad \text{(D2)}$$

We note that $T_b \cong GTA_{(G\text{-}NH)}$. Therefore, we can write as the following:

$$\hat{T}_G = (T_a + T_b)/\sqrt{2} \quad \text{(D3)}$$

$$\hat{T}_{NH} = (T_a - T_b)/\sqrt{2} \quad \text{(D4)}$$

Here, we define $T_c(\theta)$ as

$$T_c(\theta) = T_a \cos\theta + T_b \sin\theta \quad \text{(D5)}$$

Clearly,

$$T_c(\theta) = \begin{cases} T_a; & \theta = 0^\circ \\ \hat{T}_G; & \theta = 45^\circ \\ T_b \cong GTA; & \theta = 90^\circ \\ -\hat{T}_{NH}; & \theta = 135^\circ \\ -T_a; & \theta = 180^\circ \end{cases} \quad \text{(D6)}$$

CPD
8, 5455–5492, 2012

We then examined the correlation ($r_s(\theta)$) between changes in solar forcing and $T_c(\theta)$ as $r_s(\theta) = \langle$solar forcing, $T_c(\theta)\rangle$ under variable θ. If the negative correlation between the $GTA_{(G\text{-}NH)}$ and solar forcings originates completely from the positive correlation between $\hat{T}_{NH}$ and solar forcing, the maximum negative correlation of $T_c(\theta)$ should occur at $\theta \geq 135^{\circ}$. In contrast, if $\hat{T}_G$ contains anti-phase components with solar forcing and thus contributes to the negative correlation between the $GTA_{(G\text{-}NH)}$ and solar forcing, the maximum negative correlation of $r_s(\theta)$ should occur in the range $45^{\circ} < \theta < 135^{\circ}$. For the past 800 yr, the maximum negative correlation occur around 114° (Table A2). The results of the GISS simulations yielded a value similar to the observed value (Table A2). Therefore, we concluded that when solar activity is stronger (weaker), $GTA_{(G\text{-}NH)}$ becomes lower (higher) due to higher (lower) NH temperatures and lower (higher) Greenland temperatures, respectively.

Appendix E

Simple numerical experiment for Greenland, NH temperatures, and $GTA_{(G\text{-}NH)}$

A trend equation was derived by polynomial regression from the $GTP_{(G+NH)}$ calculated from the NH temperatures by Mann et al. (2009) and the Greenland temperature (Kobashi et al., 2010) (Fig. 6). Values for each year were generated from the trend equation for a period of 1200–2000. These values "*trend*" were multiplied by 1.3. Then, the random numbers that were greater than or equal to 0 and less than 1, were generated, and multiplied by 8. Then, these random numbers were added to the *trend* to produce "*seed*" time series. Synthetic NH temperature was produced by adding the *seed* to the standardized solar signal (solar 2 in Fig. 3) multiplied by two. Then, the synthetic NH temperature was smoothed by 11-yr RMs, and standardized. Synthetic Greenland temperature was generated by adding negative solar signals (multiplied by 3) to the synthetic NH temperatures. Then, the synthetic Greenland temperature

CPD
8, 5455–5492, 2012

was smoothed by 11-yr RMs, and standardized. Synthetic $GTA_{(G\text{-}NH)}$ was calculated by subtracting the standardized NH temperature from the standardized Greenland temperature. Synthetic $GTP_{(G+NH)}$ was calculated by adding the standardized NH temperature and the standardized Greenland temperature. All the coefficients were obtained to match the observed temperature records.

Appendix F

Description of the GISS-ER model and the simulations

The GISS model used in this study is the coupled atmosphere-ocean climate model GISS-ER used in the CMIP3 simulations performed for the IPCC AR4 (Schmidt et al., 2006). The model was run at 4×5 degrees of horizontal resolution with 23 vertical layers (many of the CMIP3 runs used a 20-layer version without gravity-wave drag but were otherwise identical). We performed a long control run to establish stable initial conditions, from which six transient runs were branched off, each extending from 850 to 1900 C.E. Solar forcing was applied across the ultraviolet, visible and infrared spectra based on scaling by wavelength versus total irradiance, as observed in modern satellite data. The total irradiance over time was based on the time series of Bard et al. (2007) derived from ^{10}Be data from South Pole ice core and by taking into account a small long-term geomagnetic modulation (Korte and Constable, 2005) and a polar enhancement factor. The amplitude was scaled to provide a top-of-the-atmosphere irradiance change of $1.1\,W\,m^{-2}$ between the Maunder Minimum and the late 20th century, corresponding to a tropopause radiative forcing of $0.38\,W\,m^{-2}$ (as in Shindell et al., 2006; Wang et al., 2005). The model also includes the ozone response to solar irradiance variations, which is parameterised from the results of prior GISS modelling using a full atmospheric chemistry simulation (Shindell et al., 2006) for computational efficiency. The results from these millennial transient simulations and those from a second set

CPD
8, 5455–5492, 2012

including doubled solar forcing magnitude performed to test the sensitivity of the climate response were also presented by Mann et al. (2009) and by Pechony and Shindell (2010).

Acknowledgement. We appreciate the in-depth discussion with M. Yoshimori and A. Abe-Ouchi. We thank B. Vinther and R. Keeling for useful discussion and J. Okuno for help creating the figures in earlier manuscripts. T. K. appreciates the continued support of J. Severinghaus with the temperature reconstruction. This project is supported by KAKENHI 23710020. The production of this paper was supported by an NIPR publication subsidy.

References

Bard, E., Raisbeck, G. M., Yiou, F., and Jouzel, J.: Solar modulation of cosmogenic nuclide production over the last millennium: comparison between ^{14}C and ^{10}Be records, Earth Planet. Sc. Lett., 150, 453–462, 1997.

Bard, E., Raisbeck, G., Yiou, F., and Jouzel, J.: Solar irradiance during the last 1200 yr based on cosmogenic nuclides, Tellus B, 52, 985–992, 2000.

Bard, E., Raisbeck, G. M., Yiou, F., and Jouzel, J.: Comment on "Solar activity during the last 1000 yr inferred from radionuclide records" by Muscheler et al. (2007), Quaternary Sci. Rev., 26, 2301–2304, 2007.

Barriopedro, D., García-Herrera, R., and Huth, R.: Solar modulation of Northern Hemisphere winter blocking, J. Geophys. Res., 113, D14118, doi:10.1029/2008JD009789, 2008.

Bjørk, A. A., Kjær, K. H., Korsgaard, N. J., Khan, S. A., Kjeldsen, K. K., Andresen, C. S., Box, J. E., Larsen, N. K., and Funder, S.: An aerial view of 80 yr of climate-related glacier fluctuations in Southeast Greenland, Nat. Geosci., 5, 427–432, doi:10.1038/NGEO1481, 2012.

Box, J. E.: Survey of Greenland instrumental temperature records: 1873–2001, Int. J. Climatol., 22, 1829–1847, 2002.

Box, J. E., Yang, L., Bromwich, D. H., and Bai, L. S.: Greenland ice sheet surface air temperature variability: 1840–2007, J. Climate, 22, 4029–4049, 2009.

Brohan, P., Kennedy, J., Harris, I., Tett, S., and Jones, P.: Uncertainty estimates in regional and global observed temperature changes: a new dataset from 1850, J. Geophys. Res., 111, D12106, doi:10.1029/2005JD006548, 2006.

CPD
8, 5455–5492, 2012

Cappelen, J.: DMI monthly Climate Data Collection 1768–2010, Denmark, The Faroe Islands and Greenland, 54 pp., 2011.
Crowley, T. J.: Causes of climate change over the past 1000 years, Science, 289, 270–277, 2000.
Cubasch, U., Voss, R., Hegerl, G., Waszkewitz, J., and Crowley, T.: Simulation of the influence of solar radiation variations on the global climate with an ocean-atmosphere general circulation model, Clim. Dynam., 13, 757–767, 1997.
Delaygue, G. and Bard, E.: Solar forcing based on Be-10 in Antarctica ice over the past millennium and beyond, in: Geophysical Research Abstracts, EGU 2009 General Assembly, EGU2009–6943, 2009.
Gao, C., Robock, A., and Ammann, C.: Volcanic forcing of climate over the past 1500 years: An improved ice core-based index for climate models, J. Geophys. Res.-Atmos., 113, D23111, doi:10.1029/2008JD010239, 2008.
Gray, L., Beer, J., Geller, M., Haigh, J., Lockwood, M., Matthes, K., Cubasch, U., Fleitmann, D., Harrison, G., and Hood, L.: Solar influences on climate, Rev. Geophys., 48, G4001, doi:10.1029/2009RG000282, 2010.
Grinsted, A., Moore, J. C., and Jevrejeva, S.: Application of the cross wavelet transform and wavelet c oherence to geophysical time series, Nonlin. Processes Geophys., 11, 561–566, doi:10.5194/npg-11-561-2004, 2004.
Häkkinen, S., Rhines, P. B., and Worthen, D. L.: Atmospheric blocking and Atlantic multidecadal ocean variability, Science, 334, 655–659, 2011.
Haigh, J. D.: A GCM study of climate change in response to the 11-year solar cycle, Q. J. Roy. Meteorol. Soc., 125, 871–892, 1999.
Hanna, E. and Cappelen, J.: Recent cooling in coastal Southern Greenland and relation with the North Atlantic Oscillation, Geophys. Res. Lett., 30, 1132, doi:10.1029/2002GL015797, 2003.
Hurrell, J. W.: Decadal trends in the North Atlantic Oscillation: regional temperatures and precipitation, Science, 269, 676–679, 1995.
Hurrell, J. W.: Influence of variations in extratropical wintertime teleconnections on Northern Hemisphere temperature, Geophys. Res. Lett., 23, 665–668, 1996.
Ineson, S., Scaife, A. A., Knight, J. R., Manners, J. C., Dunstone, N. J., Gray, L. J., and Haigh, J. D.: Solar forcing of winter climate variability in the Northern Hemisphere, Nat. Geosci., 4, 753–757, 2011.

CPD
8, 5455–5492, 2012

Ito, H. and Minobe, S.: Data analysis for meteorology and physical oceanography, Meteorological Research Note, 233, Meteorological Society of Japan, 263 pp., 2010.
Jones, P., Jonsson, T., and Wheeler, D.: Extension to the North Atlantic Oscillation using early instrumental pressure observations from Gibraltar and South-West Iceland, Int. J. Climatol., 17, 1433–1450, 1997.
Kobashi, T., Severinghaus, J. P., and Kawamura, K.: Argon and nitrogen isotopes of trapped air in the GISP2 ice core during the Holocene epoch (0–11, 600 B.P.): Methodology and implications for gas loss processes, Geochim. Cosmochim. Acta, 72, 4675–4686, 2008.
Kobashi, T., Severinghaus, J. P., Barnola, J. M., Kawamura, K., Carter, T., and Nakaegawa, T.: Persistent multi-decadal Greenland temperature fluctuation through the last millennium, Climatic Change, 100, 733–756, 2010.
Kobashi, T., Kawamura, K., Severinghaus, J. P., Barnola, J.-M., Nakaegawa, T., Vinther, B. M., Johnsen, S. J., and Box, J. E.: High variability of Greenland surface temperature over the past 4000 years estimated from trapped air in an ice core, Geophys. Res. Lett., 38, L21501, doi:10.1029/2011GL049444, 2011.
Kobashi, T., Kawamura, K., Goto-Azuma, K., Box, J. E., Gao, C.-C., and Nakaegawa, T.: Causes of Greenland temperature variability over the past 4000 yr: implications for northern hemispheric temperature change, Clim. Past Discuss., 8, 4817–4883, doi:10.5194/cpd-8-4817-2012, 2012.
Kodera, K.: Solar cycle modulation of the North Atlantic oscillation – implication in the spatial structure of the NAO, Geophys. Res. Lett., 29, 59–51, 2002.
Kodera, K. and Kuroda, Y.: Dynamical response to the solar cycle, J. Geophys. Res., 107, 4749, doi:10.1029/2002JD002224, 2002.
Korte, M. and Constable, C.: The geomagnetic dipole moment over the last 7000 years – new results from a global model, Earth Planet. Sc. Lett., 236, 348–358, 2005.
Kuroda, Y. and Kodera, K.: Effect of solar activity on the polar-night jet oscillation in the Northern and Southern Hemisphere winter, J. Meteorol. Soc. Jpn., 80, 973–984, 2002.
Lean, J., Beer, J., and Bradley, R.: Reconstruction of solar irradiance since 1610: implications for climate change, Geophys. Res. Lett., 22, 3195–3198, 1995.
Lean, J. and Rind, D.: How natural and anthropogenic influences alter global and regional surface temperatures: 1889 to 2006, Geophys. Res. Lett, 35, L18701, doi:10.1029/2008GL034864, 2008.

CPD
8, 5455–5492, 2012

Livingston, W. and Penn, M.: Are sunspots different during this solar minimum?, Eos, 90, 257, doi:10.1029/2009EO300001, 2009.
Mann, M. E., Zhang, Z., Rutherford, S., Bradley, R. S., Hughes, M. K., Shindell, D., Ammann, C., Faluvegi, G., and Ni, F.: Global signatures and dynamical origins of the Little Ice Age and Medieval Climate Anomaly, Science, 326, 1256–1260, 2009.
Meehl, G. A., Stocker, T. F., Collins, W. D., Friedlingstein, P., Gaye, A. T., Gregory, J. M., Kitoh, A., Knutti, R., Murphy, J. M., Noda, A., Raper, C. B., Watterson, I. G., Weaver, A. J., and Zhao, Z.-C.: Global climate projections, in: Climate Change 2007: the Physical Science Basis; Working Group I; contribution to the Fourth Assessment Report of the Intergovernmental Panel on Climate Change, Cambridge University Press, Cambridge, 747–845, 2007.
Moberg, A., Sonechkin, D. M., Holmgren, K., Datsenko, N. M., and Karlen, W.: Highly variable Northern Hemisphere temperatures reconstructed from low- and high-resolution proxy data, Nature, 433, 613–617, 2005.
Osborn, T. J.: Winter 2009/2010 temperatures and a record-breaking North Atlantic Oscillation index, Weather, 66, 19–21, 2011.
Pechony, O. and Shindell, D.: Driving forces of global wildfires over the past millennium and the forthcoming century, P. Natl. Acad. Sci., 107, 19167–19170, 2010.
Rimbu, N. and Lohmann, G.: Winter and summer blocking variability in the North Atlantic region – evidence from long-term observational and proxy data from southwestern Greenland, Clim. Past, 7, 543–555, doi:10.5194/cp-7-543-2011, 2011.
Schmidt, G. A., Ruedy, R., Hansen, J. E., Aleinov, I., Bell, N., Bauer, M., Bauer, S., Cairns, B., Canuto, V., and Cheng, Y.: Present-day atmospheric simulations using GISS ModelE: Comparison to in situ, satellite, and reanalysis data, J. Climate, 19, 153–192, 2006.
Severinghaus, J. P., Sowers, T., Brook, E. J., Alley, R. B., and Bender, M. L.: Timing of abrupt climate change at the end of the Younger Dryas interval from thermally fractionated gases in polar ice, Nature, 391, 141–146, 1998.
Shindell, D. T., Schmidt, G. A., Mann, M. E., Rind, D., and Waple, A.: Solar forcing of regional climate change during the Maunder Minimum, Science, 294, 2149–2152, 2001.
Shindell, D. T., Faluvegi, G., Miller, R. L., Schmidt, G. A., Hansen, J. E., and Sun, S.: Solar and anthropogenic forcing of tropical hydrology, Geophys. Res. Lett., 33, L24706, doi:10.1029/2006GL027468, 2006.
Steinhilber, F., Beer, J., and Fröhlich, C.: Total solar irradiance during the Holocene, Geophys. Res. Lett., 36, L19704, doi:10.1029/2009GL040142, 2009.

CPD
8, 5455–5492, 2012

Trouet, V., Esper, J., Graham, N. E., Baker, A., Scourse, J. D., and Frank, D. C.: Persistent positive North Atlantic Oscillation mode dominated the medieval climate anomaly, Science, 324, 78–80, 2009.

Vinther, B. M., Johnsen, S. J., Andersen, K. K., Clausen, H. B., and Hansen, A. W.: NAO signal recorded in the stable isotopes of Greenland ice cores, Geophys. Res. Lett, 30, 1387, doi:10.1029/2002GL016193, 2003.

Vinther, B. M., Jones, P. D., Briffa, K. R., Clausen, H. B., Andersen, K. K., DahlJensen, D., and Johnsen, S. J.: Climatic signals in multiple highly resolved stable isotope records from Greenland, Quarternary Sci. Rev., 29, 522–538, 2010.

Wang, Y. M., Lean, J., and Sheeley Jr., N.: Modeling the sun's magnetic field and irradiance since 1713, Astrophys. J., 625, 522–538, 2005.

Wanner, H., Brönnimann, S., Casty, C., Gyalistras, D., Luterbacher, J., Schmutz, C., Stephenson, D. B., and Xoplaki, E.: North Atlantic Oscillation – concepts and studies, Surv. Geophys., 22, 321–381, 2001.

Waple, A., Mann, M., and Bradley, R.: Long-term patterns of solar irradiance forcing in model experiments and proxy based surface temperature reconstructions, Clim. Dynam., 18, 563–578, 2002.

Woollings, T., Lockwood, M., Masato, G., Bell, C., and Gray, L.: Enhanced signature of solar variability in Eurasian winter climate, Geophys. Res. Lett., 37, L20805, doi:10.1029/2010GL044601, 2010.

CPD
8, 5455–5492, 2012

Table A1. The periods of stronger and weaker solar output over the past 800 yr.

#	Solar output	Top	Bottom	Duration
1	Strong	2000	1826	175
2	Weak	1825	1800	26
3	Strong	1799	1740	60
4	Weak	1739	1625	115
5	Strong	1624	1597	28
6	Weak	1596	1396	201
7	Strong	1395	1345	51
8	Weak	1344	1270	75
9	Strong	1269	1200	70

CPD
8, 5455–5492, 2012

Table A2. Degrees (θ) of the maximum negative correlation coefficients, $r_s(\theta)$, in various settings. The 95 % confidence intervals (2σ) are shown for the past 800 yr with the $\hat{T}_{NH}$ from Moberg et al. (2005) and Mann et al. (2009), including uncertainties in Greenland temperature and the NH temperature. For the past 800 yr, two sets of solar forcing were used: (a) the dataset from Bard et al. (2000) and Crowley (2000) spliced into that of Lean et al. (1995), and (b) the data set from Delaygue and Bard (2009) spliced into that of Wang et al. (2005), as shown in Fig. 3.

Datasets	Degrees (θ) of maximum negative correlation, $r_s(\theta)$
Past 161 yr (observational)	129°
Past 1000 yr; $\hat{T}_{NH}$ by Moberg et al. (2005)	(a) 111.7 ± 1.0°; (b) 111.7 ± 1.1°
Past 1000 yr; $\hat{T}_{NH}$ by Mann et al. (2009)	(a) 113.8 ± 0.8°; (b) 113.9 ± 0.9°
Simulated past 1000 yr; GISS (ensemble)	114°

CPD
8, 5455–5492, 2012

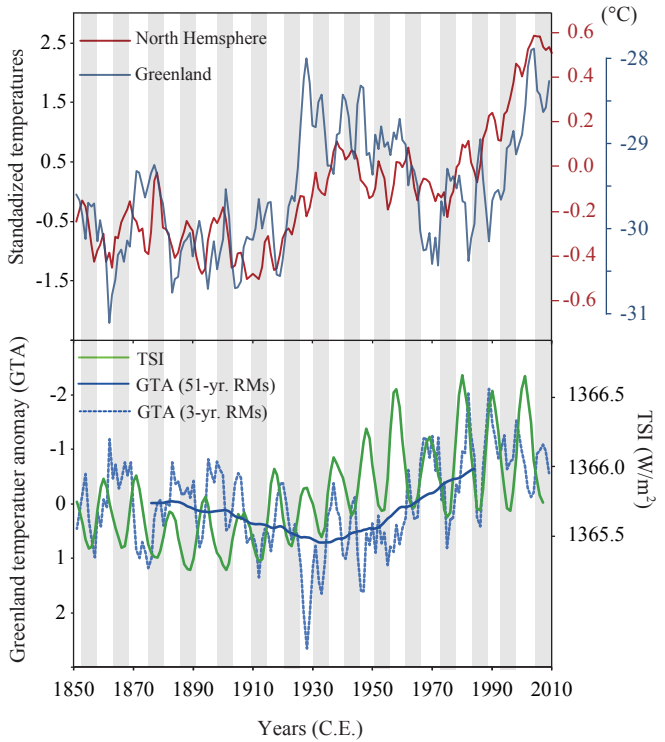

Fig. 1. Climate records for the 1850–2010 period. Top panel: annual average Greenland Summit temperature (Box et al., 2009) and annual average NH temperature (HadCRUT3) (Brohan et al., 2006). Twenty-yr root mean squared errors (RMSE) for the Summit temperature are estimated to be less than 1.6 ˚C (Box et al., 2009). Bottom panel: Greenland temperature anomaly ($GTA_{(G\text{-}NH)}$) vs. TSI (with background) (Wang et al., 2005). All time series are smoothed by 3-yr RMs except the Greenland temperature in 51-yr RMs. Shaded areas are periods of low solar activity.

CPD
8, 5455–5492, 2012

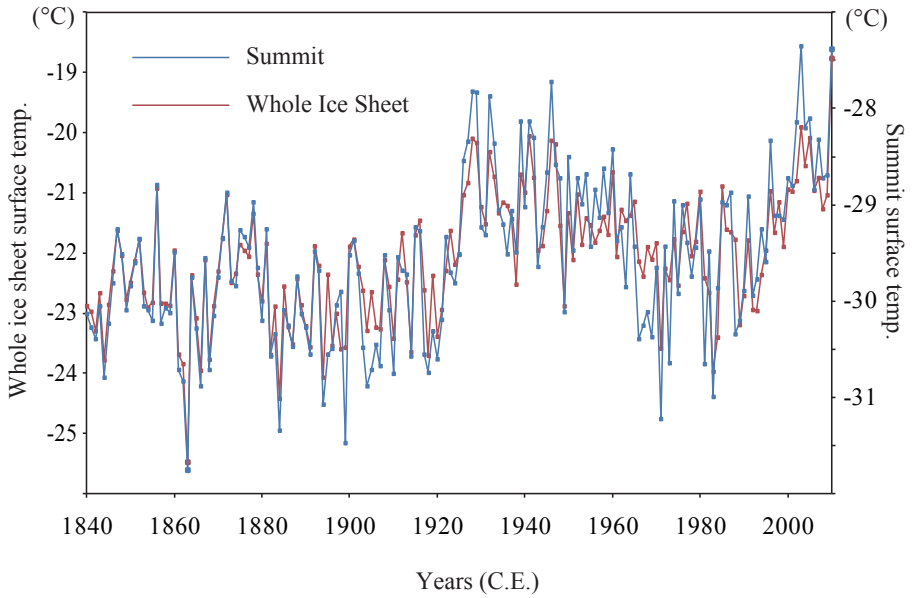

Fig. 2. The Greenland Summit surface air temperature and the whole Greenland ice sheet surface temperature were reconstructed for the last 170 yr from a spatial-temporal data fusion between the output of a regional climate model (Polar MM5) (Box et al., 2009) and in situ observations (Kobashi et al., 2011).

CPD
8, 5455–5492, 2012

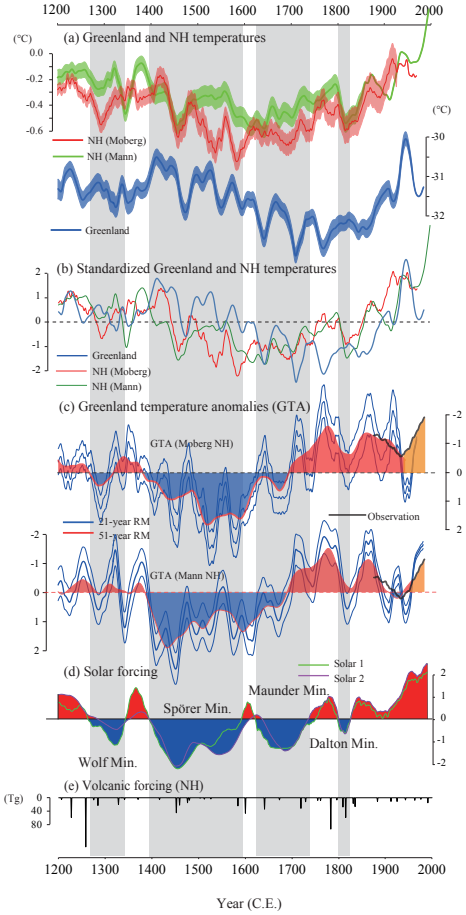

Fig. 3. Caption on next page.

CPD
8, 5455–5492, 2012

Fig. 3. Climate records for the 1200–2010 period. **(a)** Greenland temperature (blue) (Kobashi et al., 2010) and the NH temperature from Moberg et al. (2005, red) and Mann et al. (2009, green) in 21 RMs with 95 % confidence intervals (2σ) (see Appendix A). **(b)** The blue line is the standardised Greenland temperature (Kobashi et al., 2010). The red and green lines are the standardised NH temperatures (Mann et al., 2009; Moberg et al., 2005). **(c)** Greenland temperature anomalies ($GTA_{(G\text{-}NH)}$) calculated from Greenland temperature and the NH temperature as shown in panel "b" The blue and red lines are smoothed by 21 RMs with 95 % confidence intervals (2σ) (see Appendix A) and by 51 RMs, respectively. The area between the red line and zero is coloured red for the region above zero and blue for the region below zero. The black line is the $GTA_{(G\text{-}NH)}$ calculated from the observed temperatures (51 RMs) in Fig. 1. Transparent orange shading indicates areas below the observed $GTA_{(G\text{-}NH)}$ (black line) and above zero. Values of 1.27 and −0.49 are added to the observed $GTAs_{(G\text{-}NH)}$ with the NHs by Moberg et al. (2005) and Mann et al. (2009), respectively to account for the differences in the average $GTAs_{(G\text{-}NH)}$ between the proxy and the observations for the overlapping period. Note that the y-axis of the $GTA_{(G\text{-}NH)}$ is reversed to allow for comparison with the solar variability. **(d)** The purple line represents the solar forcing from Bard et al. (2000) and Crowley (2000) spliced into that from Lean et al. (1995), and the green line is from Delaygue and Bard (2009) spliced into that from Wang et al. (2005). The areas are coloured red when the values are above zero (stronger sun) and blue when the values are below zero (weaker sun). The standardised time series of the solar forcings is shown. The grey areas are the periods of weaker suns used for the statistical tests (see Appendix C). **(e)** The volcanic forcing for the NH from Gao et al. (2008) is plotted as a reference.

CPD
8, 5455–5492, 2012

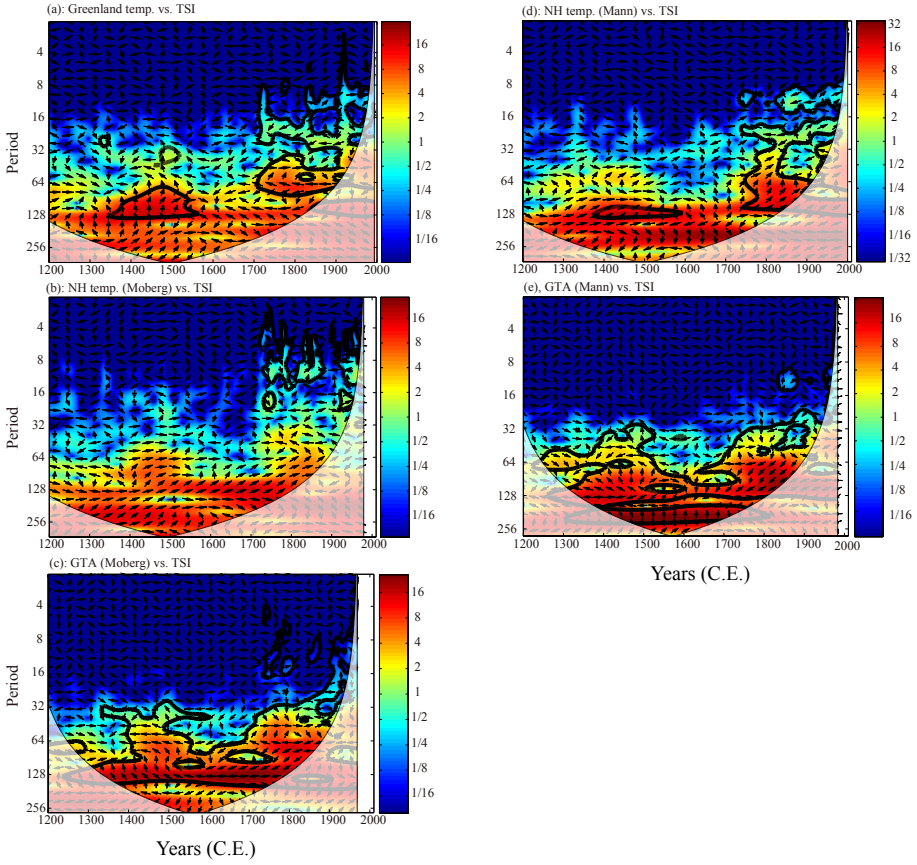

Fig. 4. Caption on next page.

CPD
8, 5455–5492, 2012

Fig. 4. Cross-wavelet transform (XWT) (Grinsted et al., 2004) of Greenland temperature, the NH temperature, the $GTA_{(G\text{-}NH)}$, and the NAO, all vs. TSI, in 1200–2010. **(a)** Greenland temperature (Kobashi et al., 2010) vs. TSI (Bard et al., 2000; Crowley, 2000; Lean et al., 1995) for 1200–2010; **(b)** the NH temperature (Moberg et al., 2005) vs. TSI (Bard et al., 2000; Crowley, 2000; Lean et al., 1995) for 1200–2010; and **(c)** the $GTA_{(G\text{-}NH)}$ with the NH temperature from Moberg et al. (2005) vs. TSI (Bard et al., 2000; Crowley, 2000; Lean et al., 1995) for 1200–2010; **(d)**, the NH temperature (Mann et al., 2009) vs. TSI (Bard et al., 2000; Crowley, 2000; Lean et al., 1995); **(e)**, the $GTA_{(G\text{-}NH)}$ (Moberg et al., 2005) vs. TSI (Bard et al., 2000; Crowley, 2000; Lean et al., 1995). Annual resolution data are used for the analyses except the $GTAs_{(G\text{-}NH)}$ that are as calculated in Appendix A. The area between the grey lines represents the 95 % confidence level relative to the noise (red). Arrows indicate relative phase relationships, with in-phase relationships denoted by right-facing arrows; arrows pointing straight down indicate that the phase of the TSI leads that of Greenland temperature, the NH temperature, or the $GTA_{(G\text{-}NH)}$ by 90°. Shaded areas represent the cone of influence where edge effects may distort the results.

CPD
8, 5455–5492, 2012

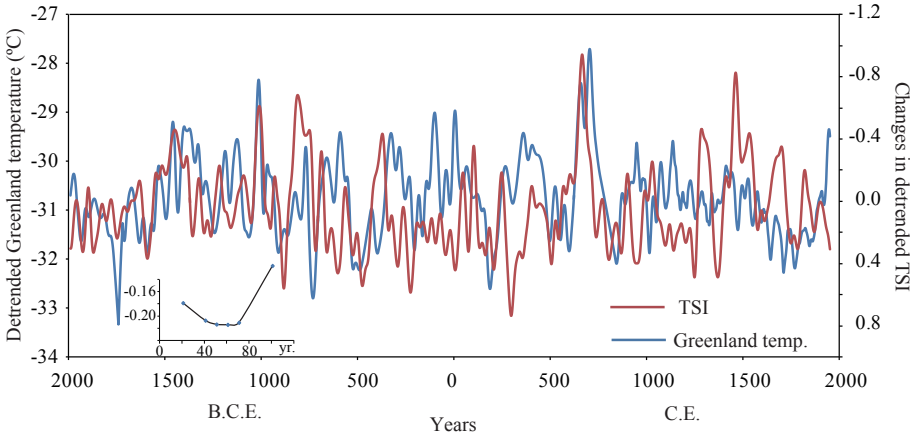

Fig. 5. Greenland temperature and solar activity over the past 4000 years. Both time series are linearly detrended and smoothed with 21-yr RMs. Greenland temperature (Kobashi et al., 2011) and solar activity (Steinhilber et al., 2009) has a weak but significant negative correlation ($r = -0.18$; $p = 0.09$). 21-yr RMs was chosen as other smoothing with various periods showed lower confidence levels although they had in some cases higher correlation coefficients (see a panel in left bottom).

CPD
8, 5455–5492, 2012

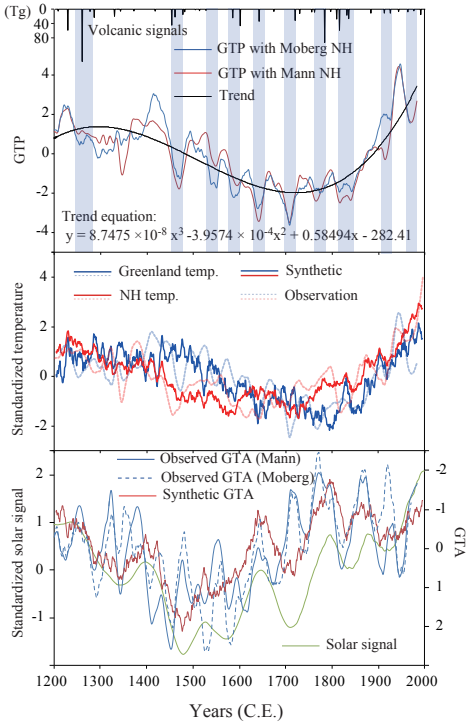

Fig. 6. Results of a simple numerical modelling. Top panel: $GTP_{(G+NH)}$ and millennial trend from polynomial regression of $GTP_{(G+NH)}$ with the NH temperature by Mann et al. (2009). The volcanic forcing for the NH from Gao et al. (2008) is plotted as a reference. Shaded areas are low GTP periods in the multi-decadal-to-centennial time scale. Note that many shaded areas coincide with large volcanic eruptions. Middle panel: synthetic and observed Greenland temperature (Kobashi et al., 2010) and NH temperature (Mann et al., 2009). Bottom panel: synthetic $GTA_{(G-NH)}$ observed $GTAs_{(G-NH)}$ with the NH temperatures by Mann et al. (2009) and Moberg et al. (2005) and standardized solar forcing (solar 2 in Fig. 2).

CPD
8, 5455–5492, 2012

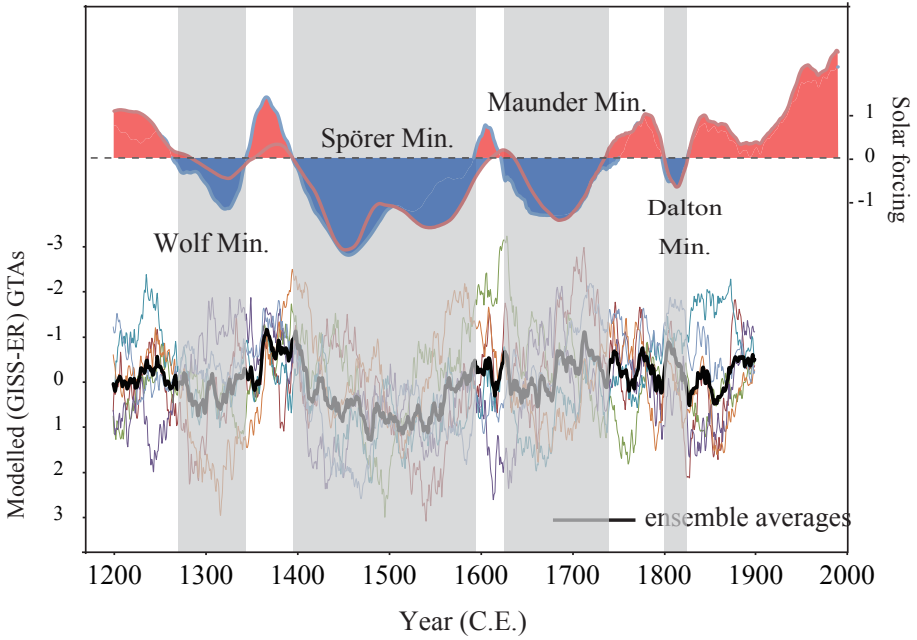

Fig. 7. Standardised solar variations (top) and $GTAs_{(G\text{-}NH)}$ in the GISS-ER simulations (bottom). The solar variations and shaded areas are the same as in Fig. 3. Thin lines in the $GTAs_{(G\text{-}NH)}$ represent each individual run and the thick black line is the ensemble averages. Note that the y-axes for the $GTAs_{(G\text{-}NH)}$ are reversed.

CPD
8, 5455–5492, 2012

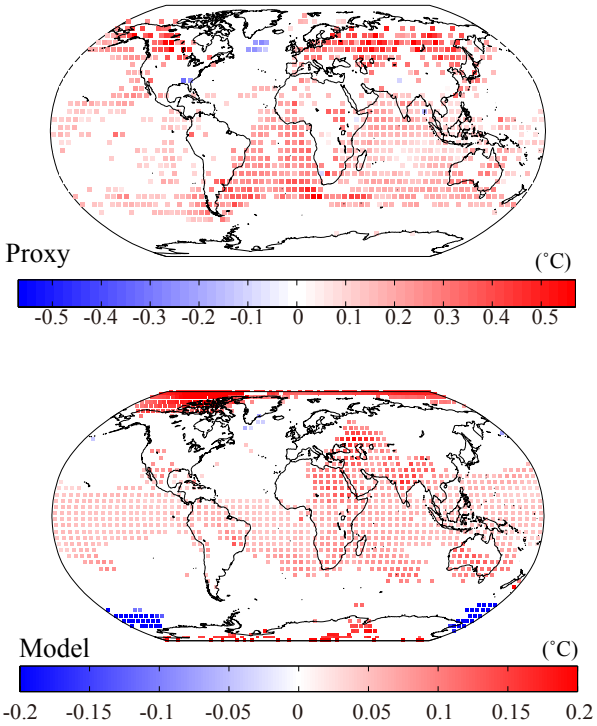

Fig. 8. Composite annual mean temperature differences (stronger solar output–weaker solar output) as defined in Fig. 3 from the model output (GISS-ER) and the proxy data (Mann et al., 2009). Only grids with 95 % significance levels (calculated by re-sampling with two-sided tests as we do not have a priori knowledge on warmer or cooler responses to solar variations except in Greenland; see Appendix C) are shown in colour. For the GISS-ER (ensemble mean result), the solar forcing from the Maunder Minimum to the late 20th century is 0.38 $W m^{-2}$ (see Appendix F).

CPD
8, 5455–5492, 2012

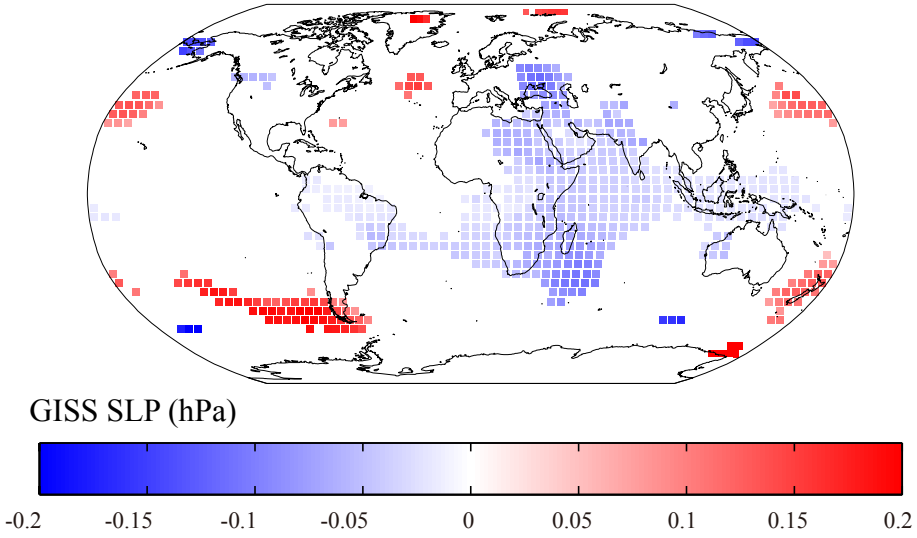

Fig. 9. Composite SLP differences in the GISS simulation (using the same data as in Fig. 8 except for the SLP). Grid data with 90 % confidence levels (calculated by re-sampling (two-sided test)) are shown in color.

CPD
8, 5455–5492, 2012

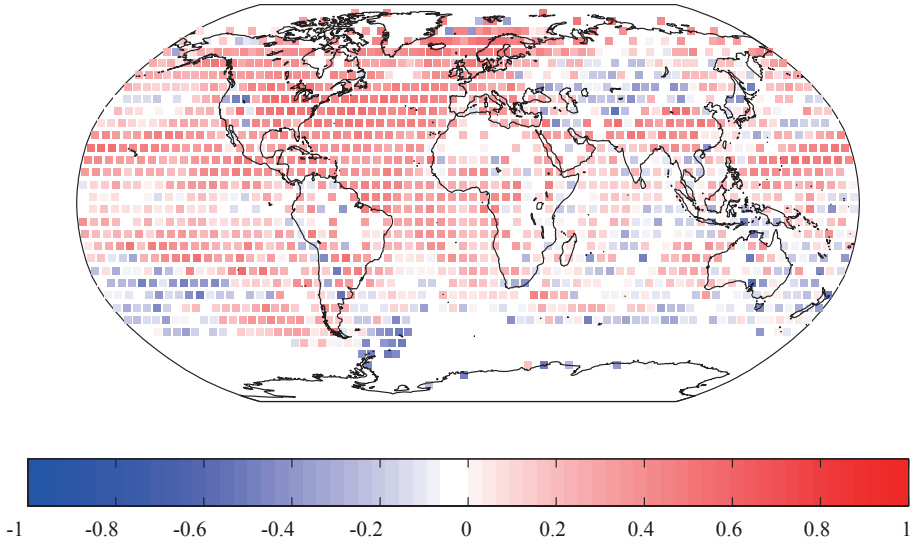

Fig. A1. Grid correlation coefficients between Greenland temperature (Kobashi et al., 2010) and the grid temperature data (Mann et al., 2009) for the 1200–1993 period. Raw data of the Greenland and NH temperature record were used for the calculation of the correlation coefficients.

CPD
8, 5455–5492, 2012